JACS
JOURNAL OF THE AMERICAN CHEMICAL SOCIETY
Article
pubs.acs.org/JACS

Free-Standing Monolayer Two-Dimensional Supramolecular Organic Framework with Good Internal Order

Martin Pfeffermann,[†] Renhao Dong,[‡] Robert Graf,[†] Wojciech Zajaczkowski,[†] Tatiana Gorelik,[§] Wojciech Pisula,[†] Akimitsu Narita,[†] Klaus Müllen,[†] and Xinliang Feng*[,‡]

[†]Max Planck Institute for Polymer Research, Ackermannweg 10, D-55128 Mainz, Germany

[‡]Center for Advancing Electronics Dresden and Department of Chemistry and Food Chemistry, Technische Universität Dresden, Mommsenstraße 4, D-01062 Dresden, Germany

[§]Institute for Physical Chemistry, Johannes Gutenberg Universität Mainz, Welderweg 11, D-55099 Mainz, Germany

Supporting Information

ABSTRACT: Utilizing dynamic self-assembly and self-sorting to obtain large-area, molecularly precise monolayered structures represents a promising approach toward two-dimensional supramolecular organic frameworks (2D SOF) or 2D supramolecular polymers. So far, related approaches suffer from small domain sizes, fragility and weak long-range internal order. Here we report on the self-assembly of a host–guest enhanced donor–acceptor interaction, consisting of a tris(methoxynaphthyl)-substituted truxene spacer, and a naphthalene diimide substituted with *N*-methyl viologenyl moieties as donor and acceptor monomers, respectively, in combination with cucurbit[8]uril as host monomer toward monolayers of an unprecedented 2D SOF. Featuring orthogonal solubility, the participating molecules self-assemble at a liquid–liquid interface, yielding exceptionally large-area, insoluble films, which were analyzed by transmission electron microscopy, atomic force microscopy and optical microscopy to be monolayers with a thickness of 1.8 nm, homogeneously covering areas up to 0.25 cm^2, and featuring the ability to be free-standing over holes of 10 μm^2. Characterization with ultraviolet–visible absorption spectroscopy, solid-state nuclear magnetic resonance spectroscopy, infrared spectroscopy, and grazing incidence wide-angle X-ray scattering allowed for confirmation of a successful complexation of all three monomers toward an internal long-range order and gave indications to an expected hexagonal superstructure. Our results extend the existing variety of two-dimensional soft nanomaterials by a versatile supramolecular approach, whereas the possibility of varying the functional monomers is supposed to open adaptability to different applications like membranes, sensors, molecular sieves, and optoelectronics.

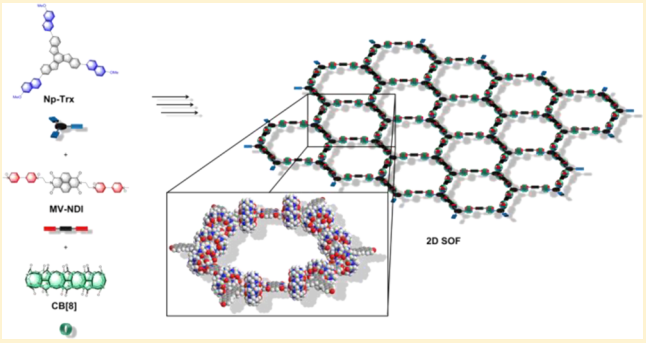

INTRODUCTION

Two-dimensional (2D) soft nanomaterials, which are defined as atomically or molecularly thin layers of atoms or molecules periodically arranged in two orthogonal dimensions,[1−3] are attracting increasing interest since the isolation of graphene as their most prominent example.[4−8] With their unique electrical, mechanical, thermal, and optical properties in combination with large surface areas, they have high potential for a variety of applications such as sensing, membranes, biotechnology, catalysis, and (opto-)electronic devices.[1,9−11] For example, free-standing monolayers of covalent organic frameworks (COFs),[6,7,12,13] as well as metal–organic frameworks (MOFs),[14−18] have recently been reported as 2D polymers and supramolecular polymers with applicability in templating,[12] photoelectric conversion,[14] and electrocatalytic hydrogen evolution.[15] Although promising results have been achieved with the networks comprising covalent bonds, 2D supramolecular polymers represent a promising approach toward molecularly precise structures over large areas.[9] Apart from the more sophisticated 2D MOFs with coordination bonds, 2D supramolecular organic frameworks (SOFs) built with other noncovalent bonds represent an incipient type of 2D supramolecular polymer. In this field, while remarkable results were already published on the assembly of 2D SOFs on liquid–solid interfaces, promoting hydrogen bonding as well as van der Waals interactions,[19−21] only a few examples comprising host–guest enhanced interactions were found to be feasible for obtaining 2D SOFs.[22−24] More precisely, host–guest enhanced interactions of dipoles[22,23] and donors and acceptors[24] by means of cucurbit[8]uril (CB[8]), respectively, have been utilized to build strong complexes. This interaction motif is able to sustain the planarity of supramolecularly interacting groups by stacking the guests face on inside the cavity of CB[8] and

Received: September 30, 2015
Published: November 3, 2015

DOI: 10.1021/jacs.5b09638
J. Am. Chem. Soc. 2015, 137, 14525−14532

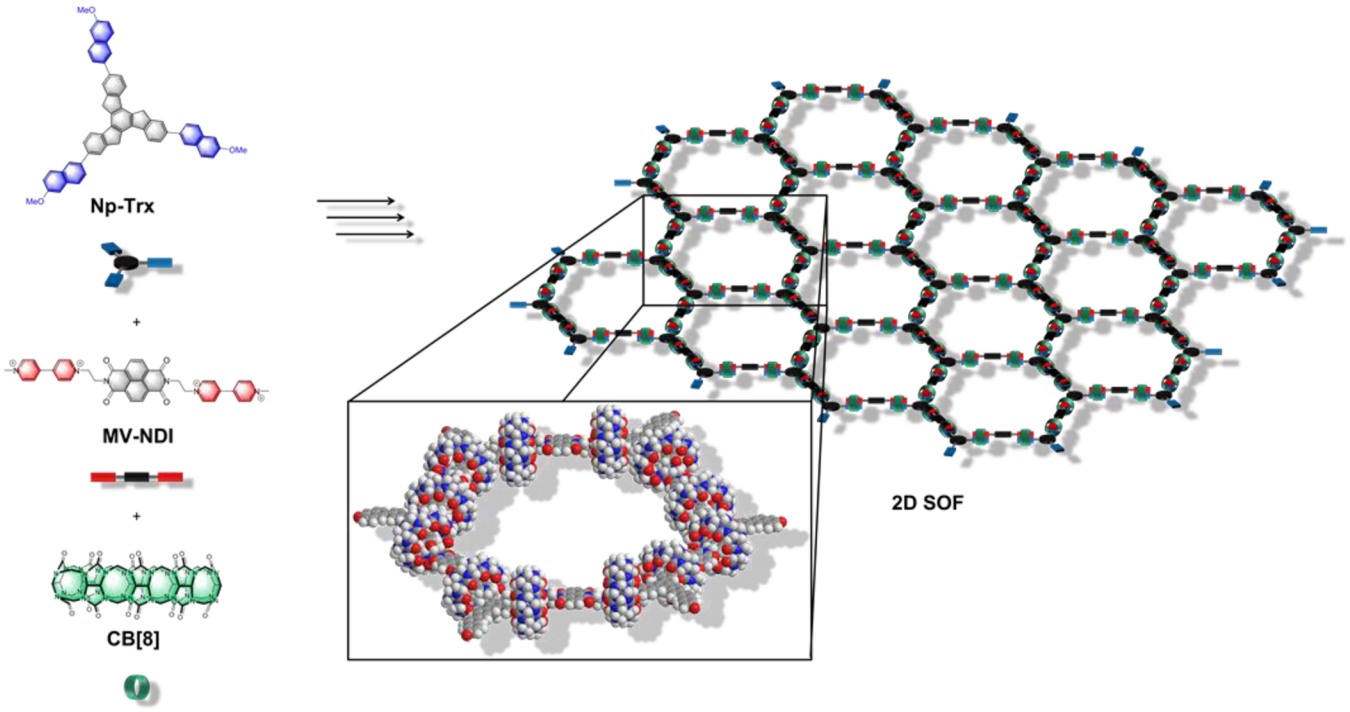

Figure 1. Schematic illustration of the assembly of the C_3-symmetric, planar donor molecule Np-Trx, the linear acceptor molecule MV-NDI, and the host-molecule CB[8] toward the hexagonal superstructure 2D SOF. The molecular structures of Np-Trx (left), MV-NDI (middle), and CB[8] (right) are shown at the top. Below each molecule, a schematic representation is visible with blue and red parts representing the donor and acceptor moieties, respectively, for visualizing the proposed superstructure. The inset represents a proposed molecular model of one hexagon of the superstructure (geometry optimized by UFF method[25]).

can therefore maintain a two-dimensional backbone of planar molecules, preventing out-of-plane polymerization.

In the case of the host–guest enhanced donor–acceptor interactions in CB[8], association constants of $K_a \geq 10^{11}$ M^{-2} were reported in literature,[26] depending on the electron affinity of participating molecules.[27] Considering the reversibility of the supramolecular assembly and its self-sorting behavior toward a thermodynamic minimum, SOFs offer a promising approach to fabricate large-area and molecularly precise 2D nanomaterials. Nevertheless, it is astounding to find thus far only a few reports on the formation of 2D SOFs, which all failed to demonstrate a long-range internal order.[22−24] To the best of our knowledge, all previous 2D SOFs were prepared in aqueous media, where they suffered from small domain sizes and low processability. Moreover, the preparation of free-standing 2D SOFs without substrate supports remains elusive, although it is imperative for their applications as membranes, for example, in ultrasensitive pressure sensors and size excluding films.[1,4,28] This is presumably due to the intrinsic defects or a limited strength of supramolecular interactions, which cannot solely sustain the SOF structures, leading to fragility.[22−24]

Herein, we report the interface synthesis and characterization of unprecedented large-area free-standing monolayers of 2D SOF, based on a host–guest enhanced donor–acceptor interaction inside CB[8]. The C_3-symmetric donor monomer Np-Trx was provided by the electron rich, planar truxene (Trx) spacer with three 6-methoxynaphthalene (Np) donor units attached to its periphery (Figure 1). The acceptor molecule MV-NDI on the other hand was obtained by connecting two *N*-methyl-4,4′-bipyridin-1-ium (MV, from *N*-methyl viologen-yl) acceptor moieties to an electron deficient naphthalene diimide (NDI). Flexible ethylene spacers were introduced between the NDI and MV units to compensate potentially occurring tensions in the expected superstructure. The electron-donating and -withdrawing spacer molecules were provided in the donor and acceptor monomer, respectively, in order to maximize the interactions and to make our 2D SOF more robust and capable of free-standing. By design, the self-assembly of donor Np-Trx and acceptor MV-NDI inside the cavity of CB[8] is expected to form a supramolecular honeycomb-network 2D SOF (Figure 1). Furthermore, to minimize tensions to the assembling 2D SOF and to prevent potentially occurring defects to result in out-of-plane polymerization, the orthogonal solubility of donor and acceptor monomers was utilized for applying the stabilizing and 2D-templating effect of a liquid–liquid interface, considering the possibility of face-on arrangements of polyaromatic hydrocarbons to an interface.[16,29] To our best knowledge, this is the first example of a 2D SOF assembled at an interface, which enabled the formation of insoluble 1.8 nm thick monolayered films of exceptionally large areas of more than 0.25 cm^2. We show an indication for successful complexation in the monolayer and provide indirect proof of successful complexation in solid state of bulk 2D SOF powder. Multilayered 2D SOF was found to comprise a long-range internal order, which is in agreement with the formation of a hexagonal arrangement of its superstructure.

RESULTS AND DISCUSSION

Synthesis of 2D SOF. The donor precursor Np-Trx was synthesized, starting with an acid catalyzed cyclotrimerization of commercially available 5-bromo-1-indanone to obtain 2,7,12-tribromotruxene[30] in 84% yield. A Suzuki coupling reaction with 6-methoxy-2-naphthaleneboronic acid gave the target

DOI: 10.1021/jacs.5b09638
J. Am. Chem. Soc. 2015, 137, 14525−14532

Scheme 1. Reaction Paths To Obtain the Donor Monomer, Np-Trx (top), and the Acceptor Monomer, MV-NDI (bottom)

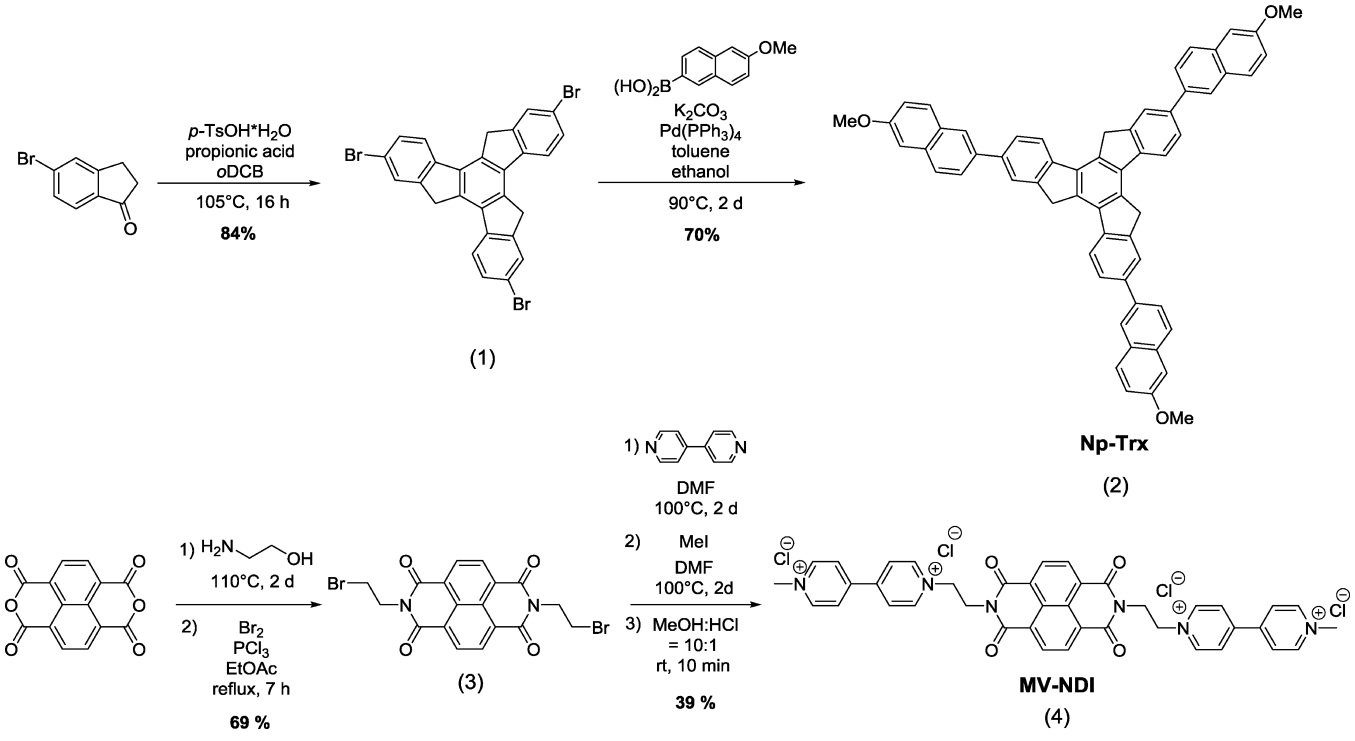

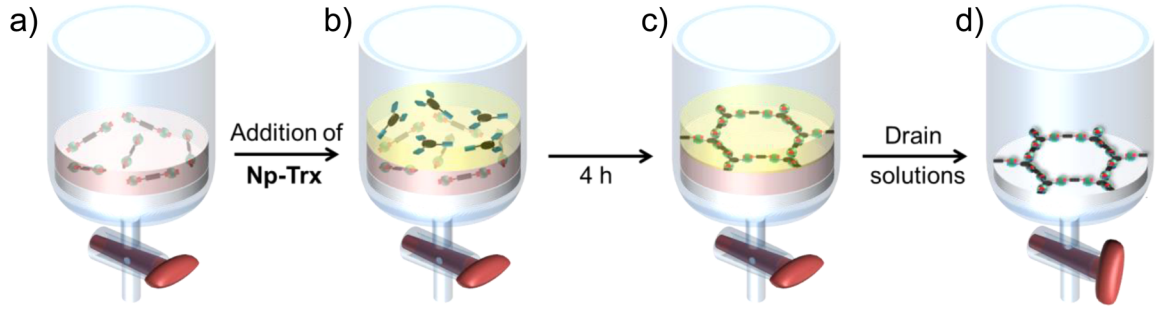

Figure 2. Schematic illustration of the self-assembly process and the deposition procedure. The pictures depict the glass trough in the different states of the process. (a) An aqueous solution of preassembled MV-NDI + CB[8] is provided. (b) The two-phase system after addition of a solution of Np-Trx in toluene is shown. (c) The self-assembled structure at the interface after an assembly time of 4 h is visible. (d) The isolated, assembled structure after draining the solutions through a valve at the bottom is illustrated.

compound Np-Trx after workup in yields of 70% (Scheme 1, top). Synthesis of the acceptor monomer MV-NDI was performed commencing with commercially available 1,4,5,8-naphthalenetetracarboxylic anhydride. Imidization with 2-aminoethanol and subsequent reaction of the crude intermediate with bromine and phosphorus trichloride gave *N*,*N*-bis(2-bromoethyl)naphthalene diimide in 69%. Introduction of *N*-methyl-4,4′-bipyridin-1-ium substituents in the periphery of *N*,*N*-bis(2-bromoethyl)naphthalene diimide was possible by nucleophilic substitution of bromide with 4,4′-bipyridine, followed by methylation with methyl iodide to obtain MV-NDI in 39% yield (Scheme 1, bottom). The molecular structure of MV-NDI, CB[8], and Np-Trx was designed to feature orthogonal solubilites, so the fabrication of 2D SOF was possible to perform at the interface of water and toluene. For initial experiments, a common liquid−liquid Langmuir−Blodgett trough was utilized for the synthesis of 2D SOF. However, due to a long time required for the assembly of the components, that is, 4 h for a monolayer, and the low vapor pressure of toluene in combination with the high surface area of the Langmuir−Blodgett trough, it was not possible to reproducibly fabricate the 2D SOF. Therefore, we turned to the use of a sealable, custom-made glass trough for the assembly and deposition process (Figure S1, SI). The trough was placed on a vibration isolation platform to avoid ruptures in the layer by peripheral vibrations. For the formation of 2D SOF, an aqueous solution of preassembled MV-NDI with CB[8] was provided in the glass trough, followed by overlaying a solution of Np-Trx in toluene (Figure 2). After the resulting interface was allowed to rest for assembly, the two-phase system was drained through the porous glass bottom, which was equipped with an appropriate substrate to allow for the deposition of the resulting insoluble 2D SOF on its surface. Following the assembly process online, for example, with a Wilhelmy-plate, was not possible, for which depositions after incremental time spans were performed and the time dependency of the resulting assembly was followed by atomic force microscopy (Figure S2, SI). The ratio of concentrations of

DOI: 10.1021/jacs.5b09638
J. Am. Chem. Soc. 2015, 137, 14525−14532

the utilized solutions was thereby found to be crucial for obtaining a continuously homogeneous layer. As the combination of MV-NDI with CB[8] in water is only able to build a dumbbell shaped complex, but not to build a macroscopic assembly without the presence of Np-Trx in toluene, the aqueous solution was applied in excess to provide a high concentration of polymerizable acceptor molecules at the interface, whereas the concentration of Np-Trx was varied to control the regularity and size of the resulting assembly. Specifically, when the concentration of Np-Trx is >4 × 10^{-5} mol/L in toluene, small fragments were obtained from the assembly process, which tended toward multilayer formation before interconnection of the fragments. In contrast, concentrations <8 × 10^{-6} mol/L resulted in connected but randomly perforated small layers. In the concentration range between 8 × 10^{-6} and 4 × 10^{-5} mol/L, homogeneous monolayers were achieved, where the concentration of 2 × 10^{-5} mol/L was found to take advantage of both a reproducible monolayer formation and a small assembly time of 4 h.

Atomic Force Microscopy (AFM), Optical Microscopy (OM), and Transmission Electron Microscopy (TEM) Studies. The assembly process over time was investigated by draining the assembling solutions onto Si/SiO_2-wafer substrates after incremental time spans and subsequent AFM analysis, which reveals separated aggregates after 1 h, small porous domains after 2 h, a continuous but defective film after 3 h, and finally a homogeneous film after 4 h (Figure S2, SI). Remarkably enough, AFM analysis on a scratched film of the 2D SOF on a SiO_2/Si-wafer, deposited after 4 h of assembly time, reveals a layer thickness of 1.8 nm (Figure 3a), which is in good agreement with the outer diameter of one CB[8] molecule[31] and complies with the height expected for CB[8]-containing polymers with CB[8] standing vertically on the substrate.[22,23] The presence of a monolayer is corroborated by persistent height differences of 1.6 nm, which were measured during monitoring the assembly process (Figure S12a–c, SI). These results thus validate that the 2D SOF has been successfully obtained as monolayer sheets. Large areas of homogeneously covered substrate were visible by OM. Figure 3b shows a picture of monolayered 2D SOF, homogeneously covering 0.25 cm^2 of Si/SiO_2 wafer substrate. In order to demonstrate the contrast with the bare substrate, the covering layer was provided with a scratch. The homogeneity of the sheet is corroborated by a small wrinkle of the layer, which is denoted with an arrow. TEM analysis of 2D SOF was carried out on lacey-carbon supported copper grids. The TEM image in Figure 3c reveals a thin free-standing film of 2D SOF homogeneously covering an area of over 200 μm^2 carbon support. The large holes in the upper region are uncovered and serve as benchmark. Remarkably, the deposited monolayer of 2D SOF was found to be free-standing on the lacey-carbon support, covering holes of sizes up to ~10 μm^2 without rupturing, suggesting a significant mechanical stability, which can be attributed to the strong supramolecular interaction in combination with a long-range order in this system. This mechanical stability is further corroborated by the canvas-like layer in Figure 3d. Although it is connected to the carbon support at only one side and one point on the opposite site, it still shows the free-standing feature. The wrinkled edge probably occurred due to strain. The small dots visible on this free-standing layer are probably dried residues from the precursor monomers. The absence of split edges in both TEM images (Figure 3c,d) further corroborates the presence of monolayered material. In accordance with other reported monolayered material,[4,32−34] our 2D SOF suffers from decomposition under high electron beam intensities, which hinders high-resolution TEM measurements to probe the molecular structure.

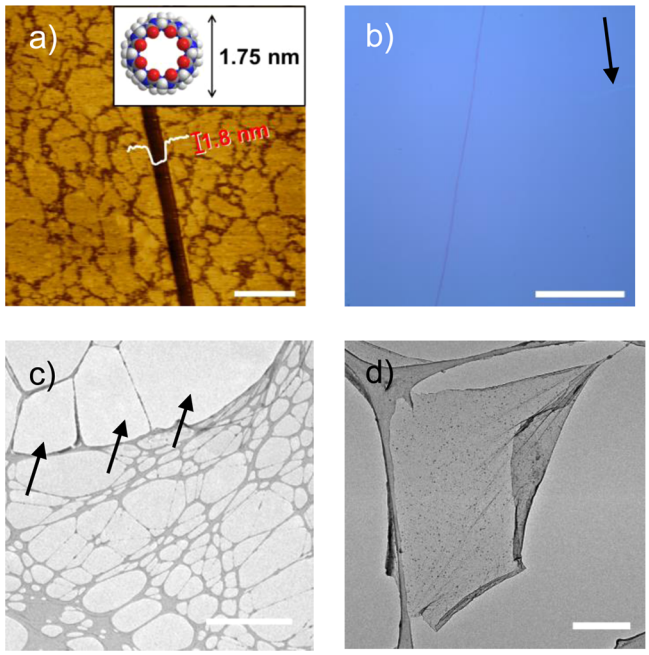

Figure 3. (a) Tapping-mode AFM height picture of the monolayered 2D SOF with a scratch. The scale bar is 1 μm. The inset shows the cross-section perpendicular to the scratch with a depth of 1.8 nm. For comparison, the molecular structure of CB[8] with an outer diameter of 1.75 nm[31] is illustrated on the right, proving the monomolecular thickness of the layer. (b) OM picture of 2D SOF, homogeneously covering a Si/SiO_2 wafer. The scratch was applied to reveal the contrast with the bare surface, and the arrow indicates a wrinkle of the layer for contrast. The scale bar is 150 μm. (c,d) TEM images of 2D SOF on lacey-carbon supported copper grids. Panel c shows a monolayer of 2D SOF, homogeneously covering large areas of the TEM grid. Arrows point out uncovered areas. The scale bar is 5 μm. (d) TEM-picture of slightly wrinkled, monolayered 2D SOF, free-standing between the lacey-carbon support. The scale bar is 2 μm.

Ultraviolet–Visible (UV–vis) and Infrared (IR) Absorption Spectroscopy. UV–vis absorption measurements were carried out on a monolayer film of 2D SOF deposited onto a quartz wafer surface (Figure 4a, black). For comparison, drop-cast films of its precursor Np-Trx and preassembled precursors MV-NDI + CB[8] were also measured on quartz wafers (Figure 4a, blue and red, respectively). Figure 4a reveals a broad absorption of the 2D SOF from 600 to 1000 nm with apparently increased absorbance with respect to its precursors, which can be assigned to a charge-transfer band of interacting donor and acceptor molecules inside CB[8].[26,35,36] This result therefore indicates the efficient complexation of monomers within 2D SOF. Notably, the absorption peaks of the NDI units at 383 and 365 nm remain unshifted in 2D SOF, suggesting that the NDI cores were not involved in the complexation. IR spectroscopy of a bulk powder (see Supporting Information for preparation) was performed on 2D SOF in comparison with its precursors for indirect proof of the stoichiometry. With IR spectroscopy not being sufficiently sensitive in its rotational–vibrational structure upon changes within this noncovalent complexation motif, one expects the spectrum of 2D SOF to be

DOI: 10.1021/jacs.5b09638
J. Am. Chem. Soc. 2015, 137, 14525–14532

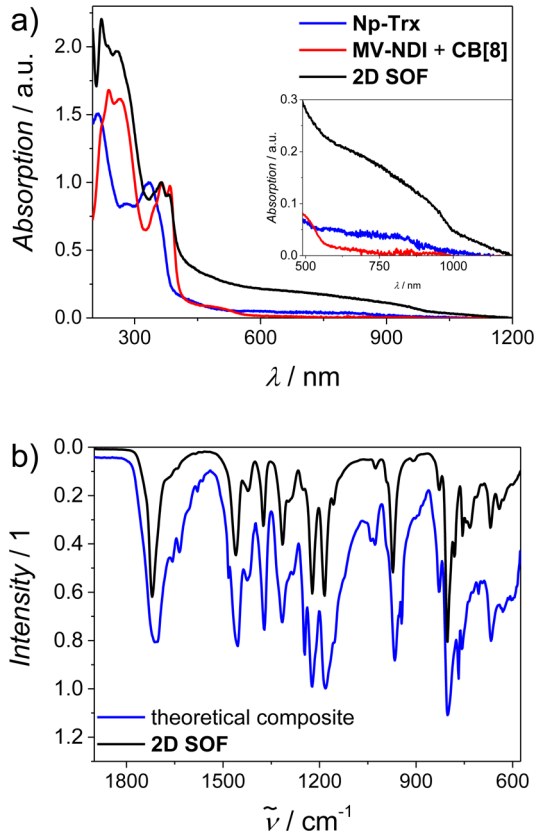

Figure 4. Solid-state characterizations of the insoluble 2D SOF. (a) Solid-state UV−vis absorption spectra of Np-Trx (blue), MV-NDI + CB[8] (red), and 2D SOF (black). To be comparable, the spectra of MV-NDI + CB[8] and 2D SOF were normalized to the 0 → 1 absorption of the naphthalene diimide spacer, and the spectrum of Np-Trx was normalized to its local maximum at 333 nm. (b) IR spectrum of 2D SOF (black) in comparison with a spectrum formed by stoichiometric superposition of those of Np-Trx, MV-NDI, and CB[8] (blue).

a stoichiometrical superposition of the individual spectra of participating components. Because the spectrum of bulk 2D SOF (Figure 4b, black) is in agreement with the stoichiometrical superposition of CB[8]/MV-NDI/Np-Trx = 6:3:2 (Figure 4b, blue), a quantitative presence of the individual components in the 2D SOF can be assumed (see Figure S3, SI for the full spectrum).

Solid-State Nuclear Magnetic Resonance (SS-NMR) Analysis. The presence of a donor−acceptor interaction of monomers was further supported by solid-state $^{13}C\{^{1}H\}$ correlation NMR spectroscopy studies. Because the amount of 2D SOF material necessary for solid state 2D $^{13}C\{1H\}$ Lee−Goldburg (LG) heteronuclear correlation (HETCOR) NMR spectroscopy was too high to be obtained by deposition of monolayers with the general procedure, we used an alternative method by stirring an aqueous solution of preassembled CB[8] and MV-NDI vigorously with a solution of Np-Trx in toluene. Thus, the liquid−liquid interface was increased and constantly renewed to obtain a larger amount of bulk 2D SOF material by filtration. Comparing the 2D $^{13}C\{^{1}H\}$ LG-HETCOR NMR spectrum of the 2D SOF (Figure 5a, black) with those of its respective precursors (Figure 5b−d; color code, see Figure 1), the correlation signals in the spectrum of the complex are shifted compared with the corresponding peaks in the correlation spectra of the precursors. The monitored chemical shift changed upon the complexation, resulting from modulations of the local electron density at the observed nuclear spin site. Therefore, decreasing chemical shift values indicate a stronger electronic shielding, which is induced by an increased electron density. Therefore, the chemical shifts of the electron donor Np-Trx can be expected to experience a low field shift upon complexation, while those of the acceptor molecule MV-NDI should clearly exhibit high field shifts at the sites involved in the complexation. The recorded $^{13}C\{^{1}H\}$ LG-HETCOR NMR spectra show correlation signals of the Np-Trx precursor between 6 and 8 ppm in the ^{1}H dimension and between 120 and 130 ppm in the ^{13}C dimension (Figure 5c, blue). These signals observe a pronounced downfield shift in both dimensions, ^{1}H as well as ^{13}C, to the resulting chemical shift values of 8−10 ppm in the ^{1}H dimension and 125−135 ppm in the ^{13}C dimension in the correlation spectrum of 2D SOF (Figure 5c, black). The strong correlation signals of MV-NDI are observed in the pure material at 9.2 ppm ^{1}H chemical shift and a ^{13}C chemical shift of 144 and 129 ppm, respectively.

In contrast to the signals of Np-Trx, the correlation signals of MV-NDI are shifted upfield to 6.7 ppm ^{1}H- and 130 ppm ^{13}C-chemical shift and 6.3 ppm ^{1}H- and 116 ppm ^{13}C chemical shift, respectively (Figure 5b). These changes in chemical shifts correspond to an increased electronic shielding of MV-NDI and a deshielding of Np-Trx, which are expected to originate from the electron donating effect of the methoxynaphthyl moiety of Np-Trx in combination with the electron withdrawing behavior of the *N*-methyl-4,4′-bipyridinyl group of MV-NDI. The changes in the signals of CB[8] upon complexation to 2D SOF (see Figure 5d) are much weaker compared with the changes in MV-NDI and Np-Trx. The correlation signal of the CH_2 groups observed at ∼55 ppm in the ^{13}C dimension as well as the carbonyl signals observed at 157 ppm in the ^{13}C dimension are almost unchanged in 2D SOF compared with pure CB[8]. Additional solid state NMR experiments probing the molecular mobility (recoupled polarization transfer heteronuclear dipolar order (REPT-HDOR) sideband patterns see Figure S14, SI) were able to reveal rigidity of the CB[8] molecules in 2D SOF, which we attribute to CB[8] hosting both acceptor and donor moieties. The correlation signals of the CB[8]-CH sites observed at 72 ppm in the ^{13}C dimension, however, reveal a heterogeneous behavior. The major contribution of the signal remains unchanged, similar to the other signals of CB[8], which is in accordance with the literature, whereas CB[8] generally exhibits only small peak shifts upon comparable complexations.[22] Nevertheless, a small fraction of CB[8] experiences a clear deshielding trend by being shifted 2 ppm in the ^{1}H and 3 ppm in the ^{13}C dimension to the low field. REPT-HDOR sideband patterns were able to contribute this signal to a CB[8] species, hosting only one guest inside its cavity (Figure S14, SI). With respect to its chemical shift, the guest is supposed to be the acceptor moiety of MV-NDI. Therefore, this fraction corresponds to defects or layer edges, which are expected in a higher amount due to the deviating preparation method of the bulk 2D SOF powder. Finally, the LG-HETCOR NMR spectrum of 2D SOF revealed very intense signals of CB[8], medium signals for MV-NDI, and only weak signals for Np-Trx, which was in qualitative agreement with the expected stoichiometry of CB[8]/MV-NDI/Np-Trx = 6:3:2 in the proposed supramolecular assembly. Even though the LG-HETCOR method is not quantitative, this stoichiometry agrees with IR spectroscopy (Figure 4b). The

DOI: 10.1021/jacs.5b09638
J. Am. Chem. Soc. 2015, 137, 14525−14532

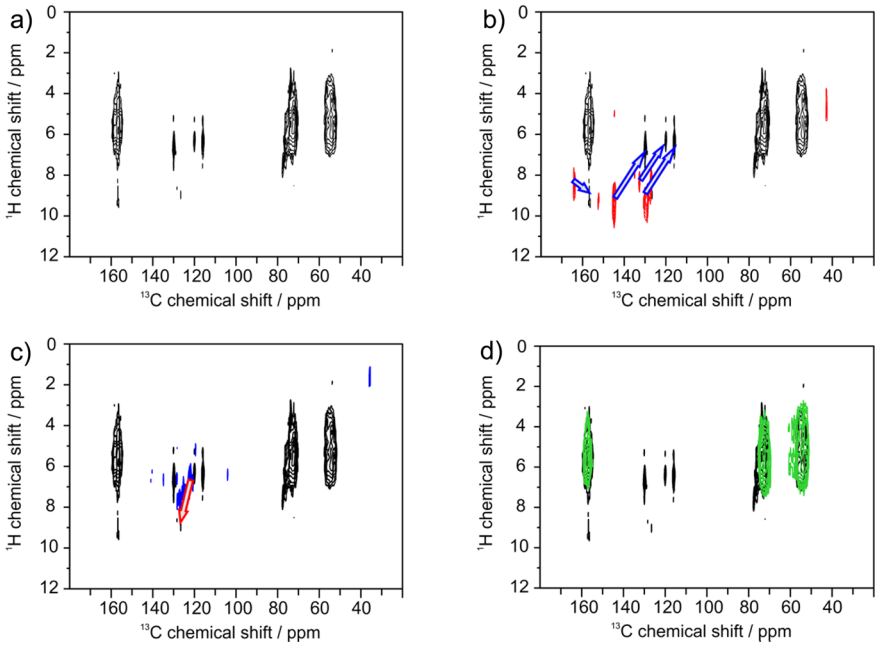

Figure 5. (a) $^{13}C\{^1H\}$ Lee–Goldburg (LG) heteronuclear correlation (HETCOR) spectrum of 2D SOF (color code, see Figure 1). In order to illustrate changes due to the complexation, superpositions of panel a with the corresponding $^{13}C\{^1H\}$ LG-HETCOR spectra of the pure precursors (b) MV-NDI, (c) Np-Trx, and (d) CB[8] are given.

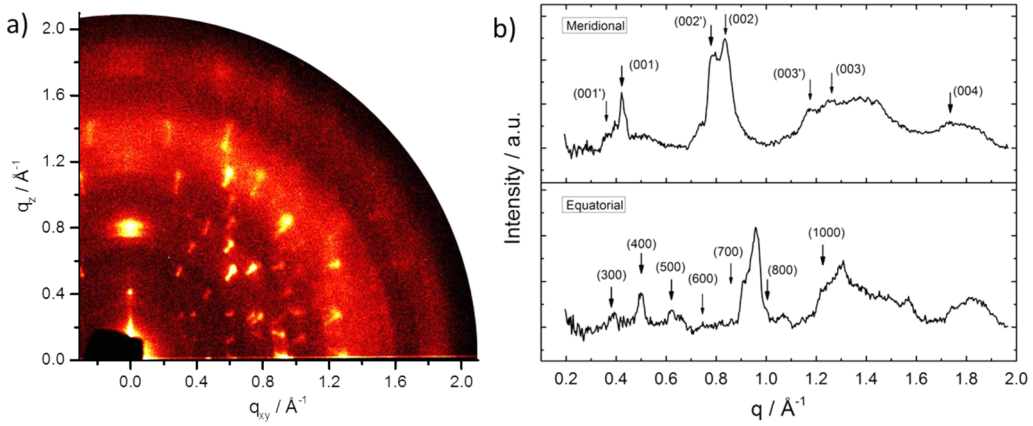

Figure 6. (a) GIWAXS pattern of a layer-by-layer deposited, 122 nm thick multilayer of 2D SOF. (b) One-dimensional integrations of the meridional (top) and the equatorial (bottom) diffractions in panel a. Arrows indicate the positions of the particular (*hkl*) scattering intensities.

visible fine structure of NMR spectra further indicates the presence of ordered structure of 2D SOF (Figure 5b–d).

Grazing Incidence Wide-Angle X-ray Scattering (GIWAXS) Analysis. So far, our attempts, including high-resolution TEM and scanning tunneling microscope (STM) experiments, were not successful to elucidate the internal structure of 2D SOF. High resolution TEM experiments suffered from a visible decomposition of the layer under the necessarily high irradiation doses, making it unfeasible to obtain the molecular structure. We attribute the unsuccessful STM experiments on the other side to a poor interaction between the 2D SOF and the substrate. With regard to CB[8] having a small contact area with the substrate's surface while standing perpendicular on the substrate, in combination with large distances between the CB[8] monomers, the 2D SOF probably suffers from a weak interaction to the substrate. The 2D SOF is therefore expected to feature high dynamics at the interface, precluding the possibility to analyze the internal structure. Thus, to gain deeper insight into the supramolecular organization within the 2D SOF layers, grazing incidence wide-angle X-ray scattering (GIWAXS) was performed. GIWAXS can provide details about the crystalline packing of weakly scattering organic materials in thin films, whereas well-ordered films typically exhibit diffraction patterns with a high number of intensive elliptical reflections.[37] In contrast to ordinary XRD measurements, GIWAXS probes the molecular packing in both in-plane (q_{xy}) and out-of-plane (q_z) directions with respect to the film surface. Conventionally, reflections along the out-of-plane and in-plane direction appearing along the q_z axis and q_{xy} axis, respectively, are indexed as (00*l*), and (*h*00) and (0*k*0), respectively. The shape, intensity, and position of diffraction peaks are related to the molecular packing within the film. Remarkably enough, the GIWAXS pattern for a 122 nm thick 2D SOF multilayer film (the preparation method was described in Supporting Information) reveals a highly ordered structure confirmed by a large number

DOI: 10.1021/jacs.5b09638
J. Am. Chem. Soc. 2015, 137, 14525–14532

of distinct reflections (Figure 6a). In order to exclude possible reflections from the precursors, their GIWAX patterns were also analyzed for comparison (Figure S4, bottom, SI). The meridional reflections of 2D SOF localized at q_z = 0.395 and 0.422 Å^{-1} (Figure 6b) correspond to *d*-spacings of 1.59 and 1.48 nm and were assigned to the (001) and (001′) interlayer planes, respectively. Following reflections up to the fourth order indicates the long-range order of the molecules in the out-of-plane direction of the film. We attribute the *d*-spacing of 1.48 nm with respect to the diameter of CB[8] of 1.75 nm[31] to a lamellar, Bernal-stacked arrangement. The splitting of the meridional reflections might be related to a marginally elliptical distortion of the CB[8] molecules, which then show two different axes along and orthogonal to the planes of the donor and acceptor moieties. The elliptical deformation of the CB[8] is in agreement with ^{13}C mobility measurements, which show a restricted rotation of CB[8] as host around its guests (Figure S14, SI). Reflections on the equatorial plane (q_{xy}) are typically a combination of two lateral packing directions and are more difficult to assign. Here we observed a pronounced periodicity, which suggests for the first visible reflection in the small-angle range at q_{xy} = 0.381 Å^{-1} the index of (300) (Figure 6b). Corresponding to a *d*-spacing of this reflection of 1.64 nm, the first order reflection along this axis then would have a *d*-spacing of 4.92 nm. A relatively simple periodic sequence of reflections point to a high symmetry of the structure within the film, which is either cubic or hexagonal according to the theoretical peak distribution derived from Bragg's law. The cubic structure, however, would contradict the symmetry of constituting molecules, which would rather adopt a hexagonal packing. Indexing the 4.92 nm reflection as (100) within a hexagonal lattice results in a unit cell parameter along this axis of 5.68 nm. The presence of peaks up to 10th order within this indexing corroborates a well-organized in-plane structure with a long-range order of molecules. The proposed hexagonal unit cell of 5.68, 5.68, and 1.5 nm is in good agreement with the 2D hexagonal structure schematically illustrated in Figure 1.

CONCLUSION

In summary, we have successfully fabricated an unprecedented 2D SOF by self-assembly of a host–guest enhanced donor–acceptor interaction in the cavity of CB[8] at a liquid–liquid interface. Monolayer films of 2D SOF with dimensions up to 0.25 cm^2 were achievable by horizontal deposition and were found to be free-standing over gaps of 10 μm^2. We attribute the homogeneity and the mechanical strength to the fundamental design of the molecules, comprising electron withdrawing and donating effects, respectively, to enhance donor–acceptor interactions in combination with an intentionally introduced flexibility to one monomer, allowing a strong complexation of the host–guest enhanced donor–acceptor interaction toward a highly regular superstructure. Although it was not possible to elucidate the internal structure unambiguously, analysis of the X-ray scattering pattern indicates the formation of a hexagonal, layered arrangement. Nevertheless, further efforts are necessary to confirm the packing model unambiguously. The regularity of the 2D superstructure in combination with the availability of free-standing monolayers makes 2D SOF most promising for applications like an ultrasensitive sensor or a size-excluding membrane. The facile, solution-based approach is readily applicable to larger scales. Regarding the feasible exchangeability of the truxene and the naphthalene diimide as implemented functional spacers, respectively, with spacer molecules of different sizes, the resulting 2D SOF derivatives are expected to be custom-tailorable to a large variety of pore sizes. Furthermore, the visible charge-transfer band in UV/vis spectroscopy indicates the rich optoelectronic properties of 2D SOF, thus paving the way for using 2D SOFs in the field of optoelectronic devices.[9,38,39]

ASSOCIATED CONTENT

Supporting Information

The Supporting Information is available free of charge on the ACS Publications website at DOI: 10.1021/jacs.5b09638.

Synthetic and experimental procedures, supplementary figures, REPT-HDOR sideband pattern, and additional GIWAXS pattern (PDF)

AUTHOR INFORMATION

Corresponding Author

*xinliang.feng@tu-dresden.de

Notes

The authors declare no competing financial interest.

ACKNOWLEDGMENTS

Financial support by the ERC grant 2DMATER and the EC under the Graphene Flagship (Grant Number CNECT-ICT-604391) are gratefully acknowledged. W.Z. acknowledges the ERC Advanced Grant NANOGRAPH (AdG-2010–267160). T.G. is grateful to DFG-Schwerpunktprogramm 1415 for the financial support. We gratefully acknowledge the beamline 9 of the DELTA electron storage ring in Dortmund for providing synchrotron radiation and technical support for GIWAXS measurements.

REFERENCES

(1) Sakamoto, J.; van Heijst, J.; Lukin, O.; Schlüter, A. D. *Angew. Chem., Int. Ed.* **2009**, *48*, 1030.
(2) Colson, J. W.; Dichtel, W. R. *Nat. Chem.* **2013**, *5*, 453.
(3) Osada, M.; Sasaki, T. *Adv. Mater.* **2012**, *24*, 210.
(4) Bauer, T.; Zheng, Z.; Renn, A.; Enning, R.; Stemmer, A.; Sakamoto, J.; Schlüter, A. D. *Angew. Chem., Int. Ed.* **2011**, *50*, 7879.
(5) Vybornyi, M.; Rudnev, A. V.; Langenegger, S. M.; Wandlowski, T.; Calzaferri, G.; Haener, R. *Angew. Chem., Int. Ed.* **2013**, *52*, 11488.
(6) Zhou, T.-Y.; Lin, F.; Li, Z.-T.; Zhao, X. *Macromolecules* **2013**, *46*, 7745.
(7) Bunck, D. N.; Dichtel, W. R. *J. Am. Chem. Soc.* **2013**, *135*, 14952.
(8) Kissel, P.; Murray, D. J.; Wulftange, W. J.; Catalano, V. J.; King, B. T. *Nat. Chem.* **2014**, *6*, 774.
(9) Zhuang, X.; Mai, Y.; Wu, D.; Zhang, F.; Feng, X. *Adv. Mater.* **2015**, *27*, 403.
(10) Kory, M. J.; Schlueter, D. A. Two-dimensional polymers, blends with thermoplastic polymers, production methods and applications. WO2015121336, Aug 20, 2015.
(11) Sun, Q.; Dai, Y.; Ma, Y.; Li, X.; Wei, W.; Huang, B. *J. Mater. Chem. C* **2015**, *3*, 6901.
(12) Baek, K.; Yun, G.; Kim, Y.; Kim, D.; Hota, R.; Hwang, I.; Xu, D.; Ko, Y. H.; Gu, G. H.; Suh, J. H.; Park, C. G.; Sung, B. J.; Kim, K. *J. Am. Chem. Soc.* **2013**, *135*, 6523.
(13) Baek, K.; Hwang, I.; Roy, I.; Shetty, D.; Kim, K. *Acc. Chem. Res.* **2015**, *48*, 2221.
(14) Sakamoto, R.; Hoshiko, K.; Liu, Q.; Yagi, T.; Nagayama, T.; Kusaka, S.; Tsuchiya, M.; Kitagawa, Y.; Wong, W. Y.; Nishihara, H. *Nat. Commun.* **2015**, *6*, 6713.
(15) Dong, R.; Pfeffermann, M.; Liang, H.; Zheng, Z.; Zhu, X.; Zhang, J.; Feng, X. *Angew. Chem., Int. Ed.* **2015**, *54*, 12058.

DOI: 10.1021/jacs.5b09638
J. Am. Chem. Soc. 2015, 137, 14525–14532

(16) Kambe, T.; Sakamoto, R.; Hoshiko, K.; Takada, K.; Miyachi, M.; Ryu, J.-H.; Sasaki, S.; Kim, J.; Nakazato, K.; Takata, M.; Nishihara, H. *J. Am. Chem. Soc.* **2013**, *135*, 2462.
(17) Garah, M. E.; Ciesielski, A.; Marets, N.; Bulach, V.; Hosseini, M. W.; Samori, P. *Chem. Commun.* **2014**, *50*, 12250.
(18) Zhao, M.; Wang, Y.; Ma, Q.; Huang, Y.; Zhang, X.; Ping, J.; Zhang, Z.; Lu, Q.; Yu, Y.; Xu, H.; Zhao, Y.; Zhang, H. *Adv. Mater.* **2015**, DOI: 10.1002/adma.201503648.
(19) Ciesielski, A.; Cadeddu, A.; Palma, C.-A.; Gorczynski, A.; Patroniak, V.; Cecchini, M.; Samori, P. *Nanoscale* **2011**, *3*, 4125.
(20) Ciesielski, A.; Palma, C.-A.; Bonini, M.; Samorì, P. *Adv. Mater.* **2010**, *22*, 3506.
(21) Garah, M. E.; Perone, R. C.; Bonilla, A. S.; Haar, S.; Campitiello, M.; Gutierrez, R.; Cuniberti, G.; Masiero, S.; Ciesielski, A.; Samori, P. *Chem. Commun.* **2015**, *51*, 11677.
(22) Zhang, K.-D.; Tian, J.; Hanifi, D.; Zhang, Y.; Sue, A. C.-H.; Zhou, T.-Y.; Zhang, L.; Zhao, X.; Liu, Y.; Li, Z.-T. *J. Am. Chem. Soc.* **2013**, *135*, 17913.
(23) Zhou, T. Y.; Qi, Q. Y.; Zhao, Q. L.; Fu, J.; Liu, Y.; Ma, Z.; Zhao, X. *Polym. Chem.* **2015**, *6*, 3018.
(24) Zhang, X.; Nie, C.-B.; Zhou, T.-Y.; Qi, Q.-Y.; Fu, J.; Wang, X.-Z.; Dai, L.; Chen, Y.; Zhao, X. *Polym. Chem.* **2015**, *6*, 1923.
(25) Kuenzel, D.; Markert, T.; Gross, A.; Benoit, D. M. *Phys. Chem. Chem. Phys.* **2009**, *11*, 8867.
(26) Rauwald, U.; Scherman, O. A. *Angew. Chem., Int. Ed.* **2008**, *47*, 3950.
(27) Rauwald, U.; Biedermann, F.; Deroo, S.; Robinson, C. V.; Scherman, O. A. *J. Phys. Chem. B* **2010**, *114*, 8606.
(28) Angelova, P.; Vieker, H.; Weber, N.-E.; Matei, D.; Reimer, O.; Meier, I.; Kurasch, S.; Biskupek, J.; Lorbach, D.; Wunderlich, K.; Chen, L.; Terfort, A.; Klapper, M.; Muellen, K.; Kaiser, U.; Goelzhaeuser, A.; Turchanin, A. *ACS Nano* **2013**, *7*, 6489.
(29) Rane, J. P.; Pauchard, V.; Couzis, A.; Banerjee, S. *Langmuir* **2013**, *29*, 4750.
(30) Amick, A. W.; Scott, L. T. *J. Org. Chem.* **2007**, *72*, 3412.
(31) Kim, J.; Jung, I.-S.; Kim, S.-Y.; Lee, E.; Kang, J.-K.; Sakamoto, S.; Yamaguchi, K.; Kim, K. *J. Am. Chem. Soc.* **2000**, *122*, 540.
(32) Payamyar, P.; Kaja, K.; Vargas, C. R.; Stemmer, A.; Murray, D. J.; Johnson, C. J.; King, B. T.; Schiffmann, F.; Van de Vondele, J.; Renn, A.; Goetzinger, S.; Ceroni, P.; Schuetz, A.; Lee, L.-T.; Zheng, Z.; Sakamoto, J.; Schlueter, A. D. *Adv. Mater.* **2014**, *26*, 2052.
(33) Zheng, Z.; Ruiz-Vargas, C. S.; Bauer, T.; Rossi, A.; Payamyar, P.; Schuetz, A.; Stemmer, A.; Sakamoto, J.; Schlueter, A. D. *Macromol. Rapid Commun.* **2013**, *34*, 1670.
(34) van Heijst, J.; Corda, M.; Lukin, O. *Polymer* **2015**, *70*, 1.
(35) Kim, H.-J.; Heo, J.; Jeon, W. S.; Lee, E.; Kim, J.; Sakamoto, S.; Yamaguchi, K.; Kim, K. *Angew. Chem., Int. Ed.* **2001**, *40*, 1526.
(36) Biedermann, F.; Scherman, O. A. *J. Phys. Chem. B* **2012**, *116*, 2842.
(37) Zhang, L.; Colella, N. S.; Liu, F.; Trahan, S.; Baral, J. K.; Winter, H. H.; Mannsfeld, S. C. B.; Briseno, A. L. *J. Am. Chem. Soc.* **2013**, *135*, 844.
(38) Zhu, W.; Zheng, R.; Fu, X.; Fu, H.; Shi, Q.; Zhen, Y.; Dong, H.; Hu, W. *Angew. Chem., Int. Ed.* **2015**, *54*, 6785.
(39) Brockway, A. M.; Schrier, J. *J. Phys. Chem. C* **2013**, *117*, 393.

DOI: 10.1021/jacs.5b09638
J. Am. Chem. Soc. 2015, 137, 14525−14532